Solid-State Electronics 92 (2014) 40–46

Contents lists available at ScienceDirect

Solid-State Electronics

journal homepage: www.elsevier.com/locate/sse

Low rate deep level transient spectroscopy - a powerful tool for defect characterization in wide bandgap semiconductors

Florian Schmidt [a,*], Holger von Wenckstern [a], Otwin Breitenstein [b], Rainer Pickenhain [a], Marius Grundmann [a]

[a] Universität Leipzig, Institut für Experimentelle Physik II, Linnéstraße 5, 04103 Leipzig, Germany
[b] Max Planck Institute of Microstructure Physics, Weinberg 2, 06120 Halle, Germany

ARTICLE INFO

Article history:
Received 29 July 2013
Received in revised form 25 October 2013
Accepted 28 October 2013

The review of this paper was arranged by Prof. E. Calleja

Keywords:
Deep-Level Transient Spectroscopy
DLTS
Defects
Low rate DLTS
Optical DLTS
ODLTS

ABSTRACT

We present an overview of implementation and application of low rate Deep-Level Transient Spectroscopy (LR-DLTS). In conventional DLTS the sensitivity of the capacitance meter must be chosen so low that the whole capacitance drift range between lowest and highest temperature can be measured. In LR-DLTS the bridge is automatically balanced (capacitance and conductivity) after each measured transient. Thus, the highest available sensitivity still avoiding an overload can be used. With LR-DLTS it is now possible to extend the rate windows to the mHz range while preserving highest possible sensitivity. This allows the detection of energetically close levels and levels with large thermal activation energy. Also low emission rates in optical DLTS can be detected this way.

1. Introduction

Deep Level Transient Spectroscopy (DLTS) is an established technique to detect electronic defects in semiconductors [1]. In the last decades many special DLTS techniques have been developed, from which ODLTS (DLTS working under permanent monochromatic light illumination [2,3]) is especially interesting for measuring optical capture cross sections (absorption spectra). For doing this, the optical emission rate must be at least in the order of the lowest experimentally accessible rate window of the DLTS system, which is for standard DLTS systems about $1\ s^{-1}$. Since the light output of monochromators is very limited, depending on the optical capture cross sections of the levels, the optical emission time constants may be well above one second, corresponding to emission rates in the mHz range. Such low rate windows are outside of the parameter range of standard DLTS systems. For detecting such low emission rates, the DLTS capacitance (*C*-) meter must work in direct current (DC) mode, hence its tuning state is not allowed to be changed during the measurement. In principle, low rate windows can be used for standard DLTS, but then the detection sensitivity is usually limited by the fact that the highest possible bridge sensitivity cannot be applied. The noise caused by choosing a low sensitivity range is basically $1/f$ noise, hence it mostly influences low rate windows.

Note that an inherent problem of all DLTS *C*-meters is the following: During a temperature (*T*-) scan the basic capacitance of the sample changes by typically 10%, and also the conductive loss changes considerably. If the tuning of the *C*-meter stays constant during the whole *T*-scan, its dynamic range must cover this large capacitance and conductance changes. This usually means that the *C*-meter is not in its most sensitive range, which is given only if both the capacitance and the conductance are perfectly tuned in the bridge circuit, and if the rf-amplification factor before demodulation is high. A permanent tuning of the *C*-meter is equivalent to working with alternating current (AC) coupling of the capacitance signal, since then the DC-part of the capacitance change would be permanently compensated to zero. In this contribution a novel *C*-meter concept is introduced, which combines high detection sensitivity with DC-coupling of the capacitance signal.

The extension of the rate window range to the mHz-range is often essential for performing meaningful ODLTS investigations. It also may allow to separate energetically neighbored levels from

* Corresponding author. Tel.: +49 341 97 32604; fax: +49 341 97 32668.
E-mail address: fschmidt@physik.uni-leipzig.de (F. Schmidt).

0038-1101/$ - see front matter © 2013 Elsevier Ltd. All rights reserved.
http://dx.doi.org/10.1016/j.sse.2013.10.021

each other, whose peaks are overlapping in the usual rate window range. Moreover, for wide bandgap materials it extends the detection range of deep levels to higher activation energies. In this contribution, after summarizing the physical basics of DLTS and ODLTS, the Low Rate DLTS (LR-DLTS) system is described in detail and typical application examples are introduced for all mentioned application fields.

2. DLTS and ODLTS

Deep Level Transient Spectroscopy (DLTS) [1,4] and Optical Deep Level Transient Spectroscopy (ODLTS) [2,3] are both based on the investigation of carrier emission from defect levels within the bandgap of semiconductors. Therefore the following transitions rates must be considered:

- the electron and hole capture rates c_n and c_p,
- the thermal and optical emission rates of trapped electrons into the conduction band, e_n and e_n^o,
- and the respective rates for hole emission into the valence band, e_p and e_p^o.

The transitions with the respective rates are shown schematically in Fig. 1.

Note that both the capture and the emission rates have been named "rates" historically, though they are not rates in the conventional sense of rate equations, having a unit of $s^{-1}\,cm^{-3}$. Instead, the "emission rate" with the unit s^{-1} is actually an *emission probability*, and only the product of the "capture rate" and the free carrier concentration is the *capture probability*. Therefore the "capture rate" is now often called *capture coefficient*. The capture rates are the product of the charge carrier flux $\Phi_{n,p}$ and the defect's capture cross-section $\sigma_{n,p}$

$$c_{n,p} = \Phi_{n,p}\sigma_{n,p}. \tag{1}$$

The capture probability is proportional to the respective capture rate coefficient, the free carrier concentration, and the mean thermal velocity $\langle v_{th}\rangle$

$$c_n = n\sigma_n\langle v_{th}\rangle_n \quad c_p = p\sigma_p\langle v_{th}\rangle_p. \tag{2}$$

For most semiconductors only one species of free carriers is present and the minority carrier concentration and its capture are negligible.

The thermal emission rates of electrons and holes are given by [5,4]

$$e_{n,p}^{th}(T) = \sigma_{n,p}^{\infty}\langle v_{th}\rangle_{n,p} g N_{c,v} \exp\left(-\frac{\Delta H}{k_B T}\right) \times \exp\left(\frac{\Delta S}{k_B}\right)\exp\left(\frac{E_{n,p}^{\infty}}{k_B T}\right). \tag{3}$$

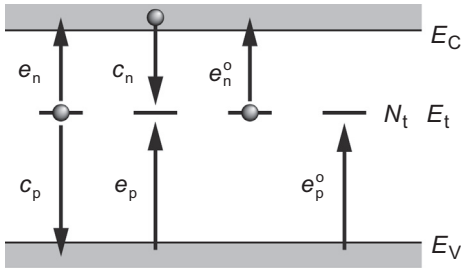

Fig. 1. Schematic depiction of the interactions of an electronic defect state with free electrons of the valence and the conduction band, respectively.

Thereby $N_{c,v}$ is the effective density of states in the conduction and valence band, g denotes the degeneracy factor, ΔH and ΔS the enthalpy and entropy change due to the transition, respectively, and $E_{n,p}^{\infty}$ the thermal capture barrier for electrons and holes. With that the apparent capture cross-section $\sigma_{n,p}$ can be written as

$$\sigma_{n,p} = \sigma_{n,p}^{\infty}\exp\left(\frac{\Delta S}{k_B}\right)\exp\left(\frac{E_{n,p}^{\infty}}{k_B T}\right). \tag{4}$$

By evaluating the entropy changes ΔS one finds the probability that the trap is occupied and with that the thermal emission rates to be

$$e_{n,p}^{th}(T) = \sigma_{n,p}\langle v_{th}\rangle_{n,p} g N_{c,v}\exp\left(\mp\frac{E_{c,v}-E_t}{k_B T}\right), \tag{5}$$

$E_{c,v}$ denoting the energetic position of the conduction and valence band edge. Similar to the capture processes, the emission rates of an optical emission process are given by [6]

$$e_{n,p}^{o}(h\nu) = \phi(h\nu)\sigma_{n,p}^{o}(h\nu), \tag{6}$$

where $h\nu$ is the photon energy, $\phi(h\nu)$ the photon flux, and $\sigma_{n,p}^{o}(h\nu)$ the defect's photon capture cross-section for electrons and holes, respectively.

While for DLTS the change of the occupancy state of the levels in the measurement phase occurs by thermal emission, ODLTS uses additional optical excitation to change the occupancy of deep defect levels within the space charge region. From Eq. (6) it is clear that the incident photon flux $\phi(h\nu)$ is essential for ODLTS investigations, because the maximum photon flux limits the experimentally accessible optical emission rate $e_{n,p}^{o}$ for a given photon energy and optical cross section. Especially for wide bandgap semiconductors large parts of the visible spectrum must be covered by the photon source used. In this work a halogen lamp was used covering a spectral range from 250 meV to 3.5 eV, which is, e.g., for the wide bandgap semiconductor ZnO exactly that part of the bandgap that cannot be investigated by thermal DLTS.

The carrier emission rate must be considered as the sum of the thermal and the optical rate,

$$e_{n,p} = e_{n,p}^{o} + e_{n,p}^{th}. \tag{7}$$

Majority carrier emission results in a decrease of the space charge region width w and with that in an increase of the diode's capacitance C. Minority carrier emission on the other hand leads to an increase of w and with that to a decrease of C. The occurrence of each capacitance transient $C(t)$ is characterized by its respective emission rate given by Eq. (7). The idea of the DLTS method [1] is to reduce the information of a single capacitance transient by an integral transformation with a suitable correlation function K to a single value S,

$$S(e_{n,p}^{o}, e_{n,p}^{th}) = \frac{1}{2\theta}\int_0^{2\theta} K(t)C(t, e_{n,p}^{o}, e_{n,p}^{th})\mathrm{d}t, \tag{8}$$

also termed DLTS signal. The time interval 2θ over which the integration is evaluated is connected with the so called "rate window" rw, which is the emission rate a level must have to maximize (minimize) S.

If we consider only the interaction between the defect level and free electrons in the conduction band for convenience, we obtain the DLTS signal S as a function of the optical and thermal emission rate as shown in Fig. 2. The maximum of S is proportional to the concentration of a deep defect, which can be emptied under optical and thermal excitation. Knowing the temperature for which the DLTS signal is maximal, enables us to determine an emission rate (Eq. (7)). A separation of $e_{n,p}^{o}$ and $e_{n,p}^{th}$ can be achieved by applying adequate measurement conditions, i.e. under dark conditions

($e^{o}_{n,p} = 0$) and for temperatures where $e^{th}_{n,p} \approx 0$. The peak of S for a given emission rate $e_{n,p}$ is obtained by applying a suitable rate window.[1] Since the experimental conditions which determine the emission rate are usually restricted (thermal degradation of the samples, limited photon flux of the light source), one can only obtain the maximum of S by applying smaller rate windows, i.e. recording longer capacitance transients.

3. The LR-DLTS setup

3.1. The C-meter

For performing LR-DLTS, a special DLTS spectrometer was used, which was developed at Max Planck Institute Halle. It combines maximum possible detection sensitivity with quasi DC-coupling. Highest possible sensitivity is given only if both the capacitance and the conductance of the sample are perfectly balanced, and if the rf-amplification before phase-sensitive rectification of the capacitance-change (ΔC) and conductance-change (ΔG) signals is maximized. Under this condition the dynamic range of the C-meter is usually low, hence during T-scan the capacitance signal will run into saturation. This can be avoided if the C-meter is continuously and slowly balanced during the T-scan, hence if the capacitance and, if possible, also the conductance balance of the C-meter are slowly regulated during the DLTS measurement in two independent feedback loops. At least the regulation of the capacitance during T-scan was realized in an early version of the SEMILAB DLTS system DLS-83, where for the compensation capacitance of the bridge a motor-driven mechanical tuning capacitor was used. This solution, however, led to disturbances in the ΔC signal whenever the motor was running, and it also did not compensate the conductance. An alternative to this solution would be to use a capacitance diode (varicap) in a slow permanent feedback loop for compensation. This feedback loop, however, acts like a high frequency pass for the ΔC signal, hence it prevents the detection of slowly changing capacitance signals. In this work an alternative bridge design is introduced, which keeps the bridge permanently close to its perfectly balanced state and nevertheless provides a DC-coupling for the ΔC signal. The capacitance measuring bridge (C-meter) is based on the resonance-tuned bridge design described in Ref. [7]. This design was extended for automatic C- and G-compensation by using a varicap and an LED-driven photoresistor. The trick for combining automatic C-tuning and d.c.-coupling of the ΔC signal is that the compensation loop is not working permanently. Instead, after each single DLTS pulse, during the DLTS measurement phase after the filling pulse, the C- and G-tuning stays constant, and only after the measurement a special "compensation step" is performed, which lasts for about 10% of the measurement time, in which C and also G are compensated. Fig. 3 shows the basic scheme of the C-meter. The sample is part of a transformer-coupled parallel resonance circuit. The varicap for C-compensation and the inductance L are the other parts of the circuit. The loss current of the circuit is balanced by the LED-driven photoresistor, which acts on a 180° phase shifted output of the transformer. In this way the bridge may be completely electronically tuned. The charge amplifier, which amplifies the bridge signal, is working at a high source impedance, which guarantees maximum detection sensitivity. On the other hand, it represents a low capacitive input impedance, which guarantees that the amplified signal is independent of the quality of the resonance circuit. The compensation trigger controls the *sample* phase of the sample and hold circuits, if it is *off* (during the C-measurement phase) the C- and G-compensation remains stable. Then the ΔC signal is really d.c.-coupled.

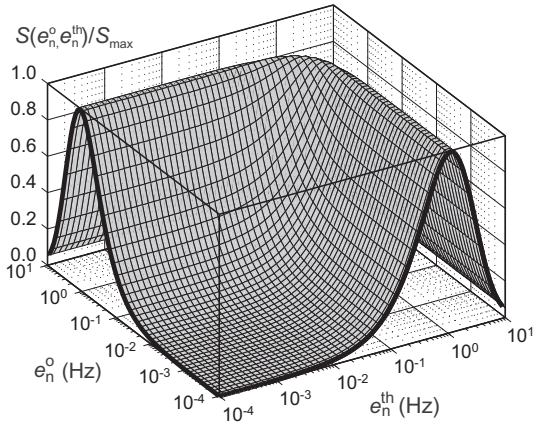

Fig. 2. The calculated DLTS signal for a deep-level showing optical and thermal emission of electrons. The signal was normalized on the peak maximum. A rate window of 1 Hz was assumed.

3.2. Principle of measurement

A schematic drawing of our LR-DLTS setup is shown in Fig. 4. It consists of a He-flow cryostat and a temperature controller both from CRYOVAC, the home-build C-meter and a computer with a DSP–FPGA-board M6713 from INNOVATIVE INTEGRATION. The M6713 board is equipped with a 300 MHz signal processor TMS320C6713 DSP from TEXAS INSTRUMENTS and four 16-bit analog digital (AD) and digital analog (DA) converters, respectively, with programmable gain and filtering working at 200 kHz. Furthermore, the board offers a dynamic 128 MB RAM memory, which is used to store the data, the measuring program and a programmable 64-bit input/output port with transistor–transistor logic for hardware control. The ODLTS measurements require an optical excitation, which is provided by a 100 W halogen lamp and a motor-driven prism monochromator SPM2 from CARL-ZEISS-JENA working with a LiF prism. For photo-current measurements as well as for the adjustment of the sample a lock-in amplifier SR810 from STANFORD RESEARCH is used.

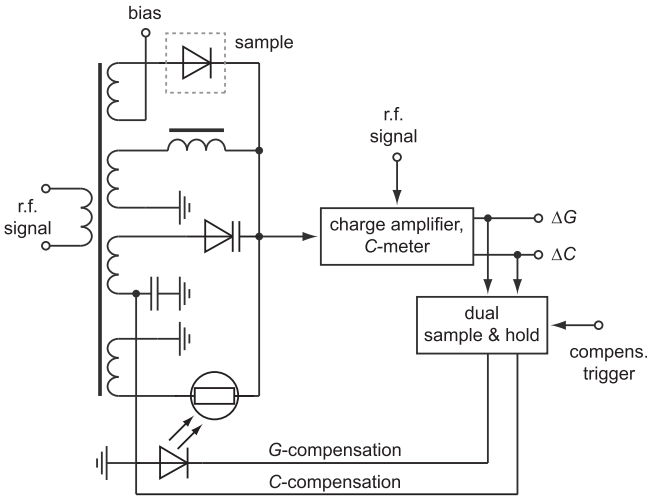

Fig. 3. Wiring diagram of the C-meter used in this setup.

[1] At the DLTS peak the product $e_{n,p} \times \theta$ is constant.

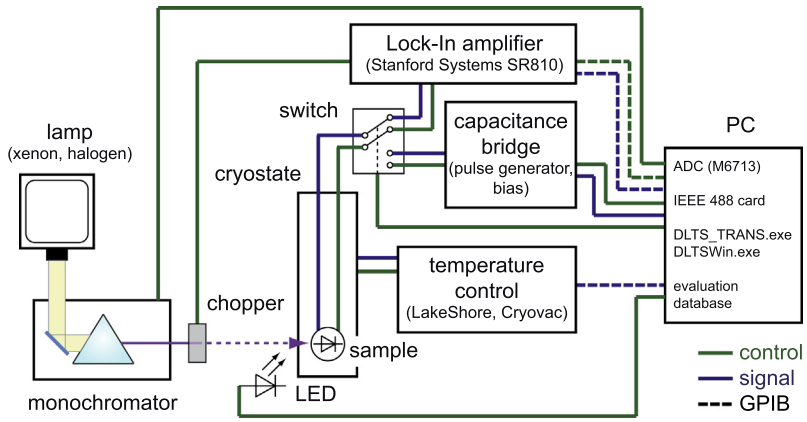

Fig. 4. Schematic illustration of the setup.

The whole setup is managed by the free-programmable board M6713. For instance the bias voltage and the pulse voltage (both max. ±10 V) are generated by the board and transferred to the *C*-meter. Furthermore, the emerging capacitance transients are collected by the card, processed, and send to the computer, where the storage and evaluation is carried out. Fig. 5 shows the workflow of a DLTS measurement. The sample is biased with a voltage V_r in reverse direction. At t_0 a filling pulse V_p is applied. The length of the filling pulse t_p is 500 ns at least. During the filling pulse the input of the charge amplifier of the *C*-meter is set to zero to avoid overload. After t_p a dead-time t_1 of typically 30 µs is waited to avoid erroneous data from the bridge. However, the dead-time is freely programmable in 5 µs steps as well. At t_2 the measurement of the transient starts. During this time (from t_1 to t_2) the dual sample and hold circuit in Fig. 4 keeps the control voltage constant. The highest data sampling rate is given by the sampling rate of the AD converter and amounts to 5 µs/sample. The measurement period for a single point can be extended by an arbitrary integer factor p, the DSP-card averages then for a time of $p \times 5$ µs. The maximum overall number of points for a single transient can be as much as $2^{15} = 32,768$. Hence the time interval the transient is recorded can be chosen arbitrary and is only be limited by the experimental conditions (e.g. temperature stability, measurement time). The sample and hold circuit in Fig. 3 is realized by a JFET transistor, a high quality capacitor, and a low-noise FET input operational amplifier. By using a digital voltmeter it was not possible to measure any drift of the output voltage over one hour. At t_3 the measurement of the transient is finished and the compensation of the bridge starts. Again this period is freely programmable, typically chosen as $t_4 - t_3 = 0.1 \times (t_3 - t_2)$, and ends at t_4, where the capacitance and conductivity measurement starts. Hence, the system records the temperature-dependent capacitance and conductance values of the sample, based on the corresponding *C*- and *G*-compensation signals. Finally, at t_0 the cycle is finished and the next cycle starts.

To improve the signal-to-noise ratio, the number of transients q, which are recorded at a certain temperature or photon energy, can be set in the measuring program. The M6713 card repeats the measurement, generates the arithmetic average of the q transients, and stores the data in a vector $\vec{T}$. Furthermore, the card calculates the integral of the averaged transients with aid of Simpson integration for each point in time (measuring point) and stores this data in a second vector $\vec{I}$. Both vectors can have 32,768 elements at most. After completion the transient-vector $\vec{T}$ and the integral-vector $\vec{I}$ are passed to the computer. The measurement process of the card is then finished.

The DLTS- or ODLTS-evaluation is done by the computer by calculating the difference of several points of $\vec{I}$ according to a given

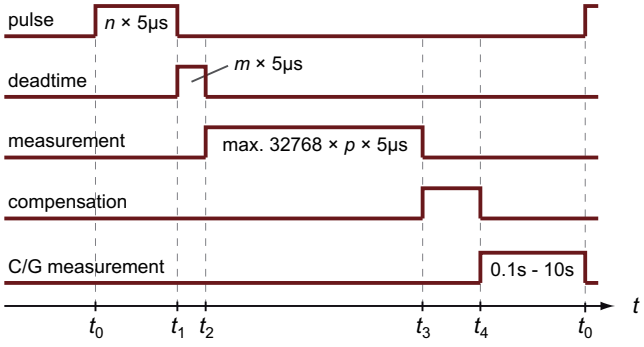

Fig. 5. Pulse sequence.

correlation function. Different emission rate-windows *rw* (for a specific correlation function) are obtained from the transients by choice of suitable time frames 2θ. The smallest possible time frame is given by the dead-time t_1 and the used correlation function. In principle there is no lower limit for the rate-window, reasonable measurement periods can be achieved with single transients being in the range of several minutes, which leads to rate-windows in the range of mHz. We notice that stable experimental conditions are crucial for the measurements of such long transients. The temperature fluctuation for instance should be below 0.1 K.

The setup opens up the possibility for further refined measuring techniques such as double DLTS, ODLTS with permanent and pulsed photon excitation, capacitance–voltage measurements, photo-capacitance measurements, and photo-current measurements. Finally it is possible to store the whole outcome of a measurement with each single transient for further external evaluation e.g. a deconvolution with aid of Laplace-DLTS [8].

4. Applications

In the following we discuss two examples for which LR-DLTS is advantageous compared to conventional DLTS. The measurements were conducted on a ZnO thin film grown via pulsed-laser deposition (PLD) on an *a*-plane sapphire substrate. A detailed description of the PLD growth setup can be found in Ref. [9]. The film has a nominal thickness of about 1 µm and was grown at 650 °C in an oxygen ambient of 0.016 mbar. Prior to the ZnO layer a highly conducting aluminum doped (1 wt%) ZnO layer was deposited, which serves as an ohmic back contact and leads to Schottky diodes with low series resistance [10]. The Schottky contacts were realized by DC reactive sputtering of palladium (Pd) with a subsequent metallic capping of Pd [11].

4.1. E3/E3′ in ZnO thin films

Within the sizeable number of electrically active defects in zinc oxide (ZnO) the E3 defect is certainly one of the most prominent. This is due to the fact, that E3 seems to be omnipresent in ZnO; it is incorporated in ZnO independent of the growth method in bulk crystals, thin films [12–24] and microwires from carbothermal evaporation [25]. The thermal activation energy E_a and the apparent capture cross-section σ determined via DLTS are reported in the range from 275 to 300 meV and from 1×10^{-16} cm^2 to about 8×10^{-16} cm^2, respectively [12–24]. However, the microscopic origin of E3 is still under debate.

By using high-resolution Laplace-DLTS [8,18] revealed that a defect labeled E3′ exists in ZnO thin films on ZnO:Al buffer causing a DLTS signal in the vicinity of that of E3. In a conventional DLTS scan recorded by using the smallest rate-windows being in the range of 1 Hz, E3′ usually occurs only as a shoulder on the high temperature side of the E3 peak; for higher rate-windows the signals of E3 and E3′ merge making the determination of the individual trap parameters difficult if not impossible.

With LR-DLTS is possible to apply rate-windows in the order of 1 mHz, for which the DLTS peaks of E3 and E3′ are shifted to lower temperatures, at which the emission rate of E3 and E3′, respectively, and with that the DLTS signals are easily distinguishable. In Fig. 6(a) a conventional thermal DLTS measurement is shown for a comparatively small rate-window of 2.4 Hz. A shoulder on the low temperature side of the E3′ signal is visible and is due to the E3 defect. The data, however, does not allow to determine trap parameters of E3′ or E3. Now, LR-DLTS extends the accessible range of emission rates by at least three orders of magnitude. With that, the signals of E3 and E3′ are measurable at temperatures for which they are clearly separated. On the basis of the LR-DLTS data an Arrhenius plot can be constructed using lineshape fits as shown by the dashed lines in Fig. 6(b) for a rate window of 76 mHz.

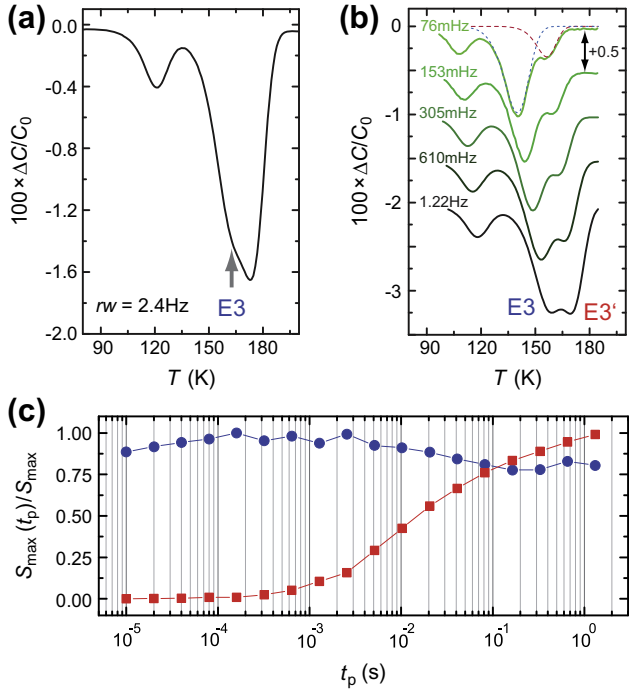

Fig. 6. (a) DLTS signal using a rate-window of 2.4 Hz and (b) rate-windows between 76 mHz and 1.22 Hz excited with a bias pulse having a length of 1280 μs. The lines in (b) have been shifted for clarity in vertical direction in equidistant steps of 0.5. (c) Normalized peak heights $S_{max}(t_p)/S_{max}$ of the E3 (circles) and E3′ (squares) peaks of a DLTS scan using a rate-window of 305 mHz as a function of filling pulse t_p.

The results of these measurements were compared with measurements performed by a dedicated Laplace-DLTS setup based on a Boonton Type 7200 capacitance bridge. Note that the pulse shapes of both setups were not the same, since the Laplace-DLTS setup shows significant ringing of the voltage after the pulses. The Laplace-DLTS spectra are shown in form of a Arrhenius contour plot in Fig. 7. Such a depiction combines the information of a conventional Arrhenius construction and the thermal emission rate distribution of the LDLTS spectra. Furthermore the Arrhenius data for E3 and E3′ obtained from the LR-DLTS measurement are included for comparison. The measurements were conducted under identical biasing conditions, i.e. using a reverse bias of 3 V and a filling pulse height of 4 V applied for 1 ms, which flattened the bands nearly completely. The trap parameters of E3 and E3′ obtained from the LR-DLTS measurement are slightly higher compared with the values obtained from the Laplace-DLTS measurement as summarized in Table 1. Data from Refs. [18,19]are similar.

Fig. 6(c) shows the DLTS peak heights $S_{max}(t_p)$ of E3 (circles) and E3′ (squares) normalized by the respective maximum peak values (S_{max}) for the same rate-window of 305 mHz. For E3′ this maximum was obtained applying a rate window of 2000 Hz and a rather long filling pulse of 10 ms. Under such conditions the DLTS peak of E3′ occurs at 210 K and the temperature-dependent capture of E3′ has saturated; the signal of E3′ is maximal. The signal heights were obtained from Laplace-DLTS measurements carried out at 160 K and are re-normalized by the saturated signal for comparison. Our results are in line with the literature data, since the electron-capture $c_n(T)$ of E3′ and with that the signal height increase for higher temperatures. Using a rate-window of 305 mHz the DLTS peak of E3′ occurs at approximately 161 K.

4.2. Optical-DLTS

As described in Section 2, optical emission rates of deep levels can be investigated by means of ODLTS. In this example we observe only an interaction between the defect and free electrons in the conduction band. This is because in our *n*-type ZnO thin film hole emission can be neglected ($e_p^{th} = e_p^o = 0$). Defects were charged using a filling pulse having the same shape and length as applied before in the conventional DLTS experiment, i.e. a reverse bias of 3 V, a filling pulse height of 4 V and a filling pulse length of 1 ms. The measurement was conducted at 300 K, where the emission

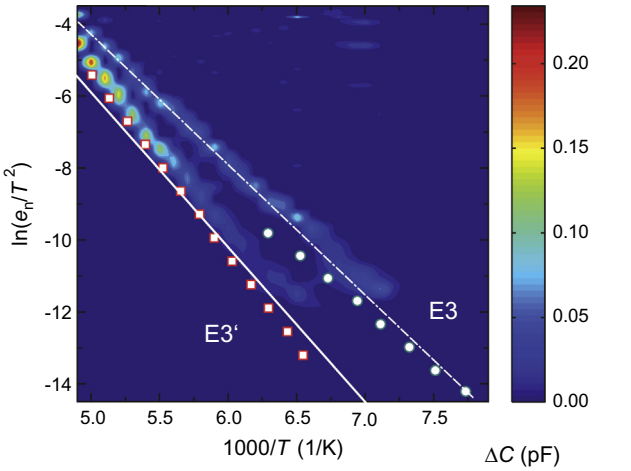

Fig. 7. Arrhenius contour plot calculated from the Laplace-DLTS spectra and Arrhenius data of E3 (circles) and E3′ (squares) obtained from the LR-DLTS measurement. The solid and dashed-doted line represents defect parameters published in Refs. [18,19], respectively.

Table 1
Trap parameters obtained from LR-DLTS and Laplace-DLTS measurements, respectively.

	LR-DLTS		Laplace-DLTS	
	E_a (meV)	σ_n (cm^2)	E_a (meV)	σ_n (cm^2)
E3	269	2.3×10^{-17}	300	5.9×10^{-16}
E3′	434	4.6×10^{-13}	362	7.7×10^{-15}

rate of E3 is too high to contribute to the DLTS signal. The concentration of E4, on the other hand, is too low and hardly visible in the thermal DLTS scan. Therefore, thermal emission processes can be neglected ($e_n^{th}\theta \approx 0$) and the emission rate during the rate window is given by e_n^o. Fig. 8(a) shows the ODLTS spectrum as a contour plot of the DLTS signal according to Eq. (8). Under illumination with photon energies of 1550 meV and 2900 meV the defects T4 [26] and TH1 [26] can be recharged, respectively, and therefore generate an ODLTS signal. The energetic position of the T4 step shows that the level is situated in the midgap region, where thermal emission processes can be excluded. Hence, the capacitance transient stems from the optical electron emission and subsequent optical hole emission of the midgap level. The TH1 defect, on the other hand, is located in the vicinity of the valence band edge. Its signal occurs due to the photo-ionization by photons with an energy above 3.1 eV and a subsequent thermal emission of the generated hole into the valence band.

The optical capture cross-section σ_n^o is determined according to Eq. (6) by the optical emission rate e_n^o and the photon flux ϕ, which is determined by the light source used and therefore usually fixed. To obtain σ_n^o in a wide energy range, it is necessary to assign the maximum ODLTS signal for each photon energy as shown exemplary for $E_{ph} = 2200$ meV in Fig. 8(b). With LR-DLTS it is possible to measure rate-windows in the mHz range and for a given photon energy $h\nu$ a by 3 orders of magnitude smaller optical emission rate and with that optical capture cross-section $\sigma_{n,p}^o$. This allows to determine $\sigma_{n,p}^o$ over a wide photon energy range. Fig. 8(c and d) show σ_n^o for T4 and TH1, respectively. The optical capture cross-section can be associated with absorption measurements and is therefore a fingerprint of a certain defect. Via the normalized peak height of the ODLTS signal $\Delta C/C_0$ and the net-doping density obtained from CV-measurements we determined the concentrations of T4 and TH1 as about 1×10^{16} cm^{-3} each. It is worth to recall that T4 and TH1 are the dominating compensating deep defects in ZnO and are not accessible with thermal DLTS.

5. Summary

In the present work we introduce an extension of the DLTS method to small rate windows down to mHz – Low Rate DLTS (LR-DLTS). By electronically re-tuning the capacitance meter (real and imaginary part) after each transient measurement event, the highest possible sensitivity range of the capacitance meter can be used without any overload, which is the presupposition to detect very slow transients with sufficient accuracy. This allows the characterization of defects in much larger energetic range below (above) the conduction (valence) band edge. Usually, the maximum temperature is practically limited by the setup or diode degradation.

For typical DLTS setup the maximum temperature is about 350 K. For this case the LR-DLTS extends the accessible energy range from 585 meV to 760 meV. In principle LR-DLTS can go to smaller rate windows if temperature stability is guaranteed. The extension of the detectable emission rates LR-DLTS also allows to construct Arrhenius plots of close lying defect states, which is not possible with conventional DLTS. This was demonstrated for the E3 and E3′ defects in ZnO. In conventional DLTS a combination of these two states appears as a single peak around 170 K. For smaller temperatures the emission rates of E3 and E3′ can be individually resolved but requires small rate windows as provided by LR-DLTS.

Optical emission rates of deep levels can be measured under external optical illumination. We showed an ODLTS measurement of a ZnO thin film with the signatures of the midgap level T4 and valence band-near defect TH1. Furthermore, we determined the optical capture cross-sections (the absorption spectra) and the concentrations of the defects. By these two examples we have shown that important information about deep level defects in wide bandgap semiconductors, which were not obtainable by conventional DLTS, can be accessed by LR-DLTS.

Acknowledgments

We thank Gabriele Ramm, Holger Hochmuth, and Michael Lorenz for preparing the PLD targets and growing the samples. To Monika Hahn, who prepared the samples, we are much obliged. This work was financially supported by the German Science Foundation (DFG) in the framework of SFB 762 (Functionality of Oxide Interfaces) and the Graduate School *Leipzig School of Natural Sciences* – BuildMoNa (GS185/1).

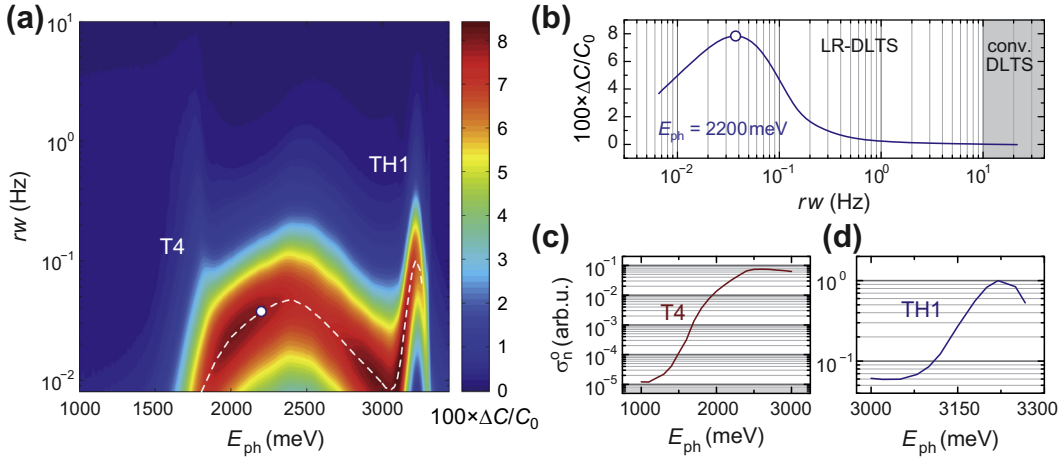

Fig. 8. (a) Contour plot of the optical DLTS measurement. The dashed line represents the position of the maximum ODLTS signal in dependence of $h\nu$. (b) Normalized ODLTS signal for a photon energy of 2200 meV. The circle represents the maximum (cf. Fig. 8(a)). (c) Optical capture cross-section of T4 and (d) TH1. Both signals were normalized on the maximum of TH1.

References

[1] Lang DV. J Appl Phys 1974;45:3023–32. http://dx.doi.org/10.1063/1.1663719.
[2] Chantre A, Vincent G, Bois D. Phys Rev B 1981;23:5335–59. http://dx.doi.org/10.1103/PhysRevB.23.5335.
[3] Brehme S, Pickenhain R. Phys Status Solidi A 1985;88:K63–6. http://dx.doi.org/10.1002/pssa.2210880160.
[4] Blood P, Orton JW. The electrical characterization of semiconductors: majority carriers and electron states. London: Academic Press; 1992.
[5] Bourgoin J, Lannoo M. Point defects in semiconductors II, Experimental aspects, vol. 35. Berlin, Heidelberg, New York: Springer-Verlag; 1983.
[6] Brehme S, Pickenhain R. Physica B 1987;145:267.
[7] Breitenstein O. Phys Status Solidi A 1982;71:159–67. http://dx.doi.org/10.1002/pssa.2210710119.
[8] Dobaczewski L, Peaker AR, Nielsen KB. J Appl Phys 2004;96:4689–728. http://dx.doi.org/10.1063/1.1794897.
[9] Lorenz M. In: Elmer K, Klein A, Rech B, editors. Transparent conductive zinc oxide: basics and applications. Springer; 2008. p. 77–122.
[10] von Wenckstern H, Biehne G, Abdel Rahman R, Hochmuth H, Lorenz M, Grundmann M. Appl Phys Lett 2006;88:092102. http://dx.doi.org/10.1063/1.2180445.
[11] Lajn A, von Wenckstern H, Zhang Z, Czekalla C, Biehne G, Lenzner J, et al. J Vac Sci Technol B 2009;27:1769–73. http://dx.doi.org/10.1116/1.3086718.
[12] Nitayama A, Sakaki H, Ikoma T. Jpn J Appl Phys 1980;19:L743–6. http://dx.doi.org/10.1143/JJAP.19.L743.
[13] Rohatgi A, Pang SK, Gupta TK, Straub WD. J Appl Phys 1988;63:5375–9. http://dx.doi.org/10.1063/1.340355.
[14] Auret FD, Goodman SA, Legodi MJ, Meyer WE, Look DC. Appl Phys Lett 2002;80:1340.
[15] Polyakov AY, Smirnov NB, Govorkov AV, Kozhukhova EA, Vdovin VI, Ip K, et al. J Appl Phys 2003;94:2895–900. http://dx.doi.org/10.1063/1.1597944.
[16] Gu QL, Ling CC, Brauer G, Anwand W, Skorupa W, Hsu YF, et al. Appl Phys Lett 2008;92:222109. http://dx.doi.org/10.1063/1.2940204.
[17] Diaconu M, Schmidt H, Hochmuth H, Lorenz M, von Wenckstern H, Biehne G, et al. Solid State Commun 2006;137:417–21. http://dx.doi.org/10.1016/j.ssc.2005.12.028.
[18] Auret FD, Meyer W, van Rensburg PJ, Hayes M, Nel J, von Wenckstern H, et al. Physica B 2007;401–402:378–81. http://dx.doi.org/10.1016/j.physb.2007.08.192. proceedings of the 24th International Conference on Defects in Semiconductors.
[19] Frank T, Pensl G, Tena-Zaera R, Zúñiga-Pérez J, Martínez-Tomás C, Muñoz-Sanjosé V, et al. Appl Phys A 2007;88:141–5. http://dx.doi.org/10.1007/s00339-007-3963-3.
[20] von Wenckstern H, Brandt M, Schmidt H, Biehne G, Pickenhain R, Hochmuth H, et al. Appl Phys A 2007;88:135–9. http://dx.doi.org/10.1007/s00339-007-3966-0.
[21] Leach C, Vernon-Parry K, Ali N. J Electroceram 2010;25:188–97. http://dx.doi.org/10.1007/s10832-010-9614-7.
[22] Simpson JC, Cordaro JF. J Appl Phys 1988;63:1781–3. http://dx.doi.org/10.1063/1.339919.
[23] Auret FD, Goodman SA, Hayes M, Legodi MJ, van Laarhoven HA, Look DC. Appl Phys Lett 2001;79:3074–6. http://dx.doi.org/10.1063/1.1415050.
[24] Han J, Mantas P, Senos A. J Eur Ceram Soc 2002;22:49–59. http://dx.doi.org/10.1016/S0955-2219(01)00241-2.
[25] Schmidt F, Müller S, von Wenckstern H, Dietrich CP, Heinhold R, Kim H-S, et al. Appl Phys Lett 2013;103:062102. http://dx.doi.org/10.1063/1.4817824.
[26] Schmidt M, von Wenckstern H, Pickenhain R, Grundmann M. Solid-State Electron 2012;75:48–54. http://dx.doi.org/10.1016/j.sse.2012.04.043.